The Company of Biologists

RESEARCH ARTICLE

Determination of the wingsnap sonation mechanism of the golden-collared manakin (*Manacus vitellinus*)

Daniel J. Bodony[1],*, Lainy Day[2], Anthony R. Friscia[3], Leonida Fusani[4,5], Aharon Karon[6], George W. Swenson, Jr[7], Martin Wikelski[8,9] and Barney A. Schlinger[10,11]

ABSTRACT

Male golden-collared manakins (*Manacus vitellinus*), small suboscine passeriform birds of Panamanian forests, communicate acoustically using a variety of non-vocal sonations. The most prominent sonations are single or multiple intense 'wingsnaps' with a dominant acoustic frequency around 5 kHz. Several hypotheses have been proposed addressing the source of the sound, ranging from purely aerodynamic origins (due to a rapid jet of air formed by the wings or by a 'whiplike' motion) to purely structural origins (such as physical contact of the wings), but without definitive assessment. Using anatomical analysis as well as high-speed video and synchronized audio recordings, we show that compared with related species, *M. vitellinus* radii are morphologically unique and confirm that they collide over the back of the bird at the moment (±1 ms) the wingsnap is produced. Using aeroacoustic theory, we quantitatively estimate the acoustic signatures from several sonation mechanisms. We conclude that only the physical contact hypothesis, wherein the wing collisions create the sound, is consistent with the measured sonation.

KEY WORDS: Sonation, Manakin, Aeroacoustics

INTRODUCTION

Animals communicate using a variety of sensory modalities with acoustic communication being the best developed in many vertebrates. Vocalizations, such as human speech and birdsong, are familiar forms of acoustic communication and the laryngeal and syringeal mechanics that produce these sounds are well studied (Riede and Goller, 2010). Many animals produce diverse non-vocal acoustic signals, termed sonations by some investigators. The mechanisms for these forms of sound production have only recently become a focus of investigation (Bostwick and Prum, 2003, 2005; Bostwick et al., 2010; Clark and Feo, 2008).

[1]Department of Aerospace Engineering, University of Illinois at Urbana-Champaign, IL 61801, USA. [2]Department of Biology, The University of Mississippi, Oxford, MS 38677, USA. [3]Department of Integrative Biology and Physiology, University of California, Los Angeles, CA 90095, USA. [4]Department of Cognitive Biology, University of Vienna, UZA 1, Biologiezentrum Althanstrasse 14, 1090 Vienna, Austria. [5]Konrad Lorenz Institute for Ethology, University of Veterinary Medicine, Savoyenstrasse 1a, A-1160 Vienna, Austria. [6]Department of Aerospace Engineering, Georgia Institute of Technology, Atlanta, GA 30313, USA. [7]Department of Electrical and Computer Engineering, University of Illinois at Urbana-Champaign, IL 61801, USA. [8]Max Planck Institute for Ornithology, Vogelwarte Radolfzell, Am Obstberg 1, 78315 Radolfzell, Germany. [9]Department of Biology, University of Konstanz, Postfach M633, 78457 Konstanz, Germany. [10]Department of Integrative Biology and Physiology, and Department of Ecology and Evolutionary Biology, University of California, Los Angeles, CA 90095, USA. [11]Smithsonian Tropical Research Institute, Roosevelt Avenue, Tupper Building – 401, Panama City 0843-03092, Panama.

*Author for correspondence (bodony@illinois.edu)

Manakins (Aves: Pipridae) are a family of neotropical birds known for their spectacular male courtship displays that include much visual and acoustic signaling (Johnsgard, 1994). In addition to vocalizing (a syringeal function in birds), males of many manakin species produce some sonations (Prum, 1998) that are tonal and whistle-like, and others that are atonal sharp cracks or snaps. These latter sounds appear to involve rapid movements of the wings and/or tail, but it is difficult to determine this definitively because the birds often inhabit field sites where study of their behavior is challenging. They are not easily held in captivity and the very rapid movements of the appendages are not readily captured using standard video recording.

Developments in understanding atonal sonations have been facilitated by the use of portable high-speed videography. For example, high-speed videos show that male club-winged manakins (*Machaeropterus deliciosus*) of Ecuador use a stridulation mechanism to produce a non-vocal high-pitched tone as specialized barbs on wing-feather shafts are brought across one another (Bostwick and Prum, 2005), much like cricket song. Male manakins of the genus *Manacus* produce a variety of conspicuous single and rolled snaps using their wings, termed 'wingsnaps' (Chapman, 1935; Snow, 1962; Schlinger et al., 2013). The mechanism for this sonation has long intrigued biologists because the amplitude of the snaps is surprisingly loud for so small a bird (∼18 g). The speed of the birds' movements is so quick that unambiguously determining the origin of the sonation is difficult. Using high-speed videography (up to 500 frames s^{-1}), Bostwick and Prum (2003) showed that wingsnaps are produced as the wings make contact over the back of the bird. Their methodology, however, did not allow them to discriminate their three hypotheses for sound production: (1) whip-like sonic waves produced by the wing (or part of the wing) moving faster than the speed of sound; (2) vacuum-created pressure claps created when a low pressure center is suddenly collapsed; or (3) percussion resulting from forceful impact of the wings. In hypotheses 1 and 2 (H1 and H2, respectively), air is used to create the sound and carry it to the microphone. In contrast, in hypothesis 3 (H3), a percussive motion creates the sound through impact.

Using high-speed videography with advances in both frame rate (1000 to 2000 frames s^{-1}) and audio-video synchronization (0.5–1.0 ms), anatomical analyses of the bones of the manakin forewing and aeroacoustic theory, we connected the kinematic motion of the wing during sonation to the motion it induces on the surrounding air and, ultimately, to the source of the sonation and determined that H1 and H2 are not consistent with the available data. Two derivative hypotheses of H2 (a and b) that examine the movement of air created by the forewing during wingsnap are also not consistent with the available data. We show that the hand clap analysis of Fletcher (2013) does not apply to manakin wingsnap because it requires a near-impermeable surface to be used during

sonation, while the clapping sounds of pigeon wings during the upstroke and downstroke (Dial, 1992) involve the collision of the primary feathers, which we do not observe in the manakin wingsnap. The percussive hypothesis (H3), wherein the radii collisions create the sound, is consistent with the measured atonal sonation.

Summary of aeroacoustic theory

To provide context for the data collection and subsequent analysis, we give a short summary of the relevant aeroacoustic theory; more information can be found in Morse and Ingard (1968) and in Goldstein (1976). Broadly speaking, sound is generated when at least one of these conditions is true: (a) an object undergoes oscillatory motion, (b) the fluid carrying the sound is unsteady or (c) an object moves supersonically. Examples of these three conditions are the beating of a drum head, the exhaust of an aircraft jet engine and the sonic boom created by a supersonically traveling aircraft, respectively. Aeroacoustic theory demonstrates the utility (see especially Goldstein, 1976) of the compactness ratio, which is defined as the ratio of the size of the object creating the sound (called the source) to the acoustic wavelength, ℓ / λ. The wavelength of the sound is related to the frequency f of the sound by $\lambda = a_\infty / f$ for sound propagating in a uniform medium of sound speed a_∞. When the compactness ratio is small, i.e. when the object creating the sound is much smaller than the wavelength of the sound it generates, it can be shown that the time history of the sound field at a point $\mathbf{x}$, denoted $p'(\mathbf{x}, t)$, follows the time history of the acoustic source. Furthermore, within the small compactness ratio limit, the mechanism for sound generation can be classified as being due to sources of mass, $Q(\mathbf{y}, t)$, or to body forces, $\mathbf{F}(\mathbf{y}, t)$, and written as (Lowson, 1965):

$$
p'(x, t) = \frac{\rho}{4\pi r} \frac{\mathrm{d}Q}{\mathrm{d}t} \bigg|_{t-r/a_\infty}
$$
$$
+ \sum_{i=1}^{3} \left[\frac{x_i - y_i}{4\pi (1 - M_r^2) a_\infty r^2} \left\{ \frac{\partial \mathbf{F}_i}{\partial t} + \frac{\mathbf{F}_i}{1 - M_r} \frac{\partial M_r}{\partial t} \right\} \right]_{t-r/a_\infty}, \quad (1)
$$

where the microphone measurements are taken at point x due to a source of sound located at point $\mathbf{y}$, separated by distance $r = |\mathbf{x} - \mathbf{y}|$. Eqn 1 has been simplified from its more general form (Goldstein, 1976) for our analysis in two ways. First, the source of sound due to an unsteady source of mass relevant for H2a does not move relative to the microphone location and has been assumed to be stationary. Second, the sound source due to unsteady forces presented in discussing H2b moves but is located at a single point $\mathbf{y}(t)$. The term:

$$
M_r = \sum_{i=1}^{3} \frac{(x_i - y_i)|\dot{\mathbf{y}}|}{r a_\infty} \quad (2)
$$

is the Mach number of the source in the direction from the source to the measurement. The subscript $t - r/a_\infty$ indicates that the sound heard at time t was generated in the past at the time required to travel from the source at point $\mathbf{y}$ to the measurement location at point $\mathbf{x}$. The remainder of the paper describes the experimental measurements and theoretical modeling undertaken to estimate the mass sources $Q(\mathbf{y}, t)$ and body forces $\mathbf{F}(\mathbf{y}, t)$ implicated in the atonal sonation hypotheses H1–H3 for *M. vitellinus*. The clear kinematics of the wings during a wingsnap event were crucial for

obtaining many of the estimates incorporated in these determinations.

MATERIALS AND METHODS
Experimental field measures

Field studies were conducted in areas of forest around Gamboa (9°07′N, 79°42′W), Province of Panama, Republic of Panama, as part of a long-term investigation into the behavioral physiology of golden-collared manakins, *Manacus vitellinus* (Gould 1843) (Schlinger et al., 2013). All procedures were authorized by the Smithsonian Tropical Research Institute, the Autoridad Nacional del Ambiente of the Republic of Panama and the UCLA Chancellors and University of Mississippi Animal Research Committees.

Behavioral variables

We focused on two mechanical sounds that *M. vitellinus* males produce during courtship displays: the single wingsnap and the rollsnap (Chapman, 1935; Snow, 1962; Skutch, 1969; Schultz and Schlinger, 1999; Bostwick and Prum, 2003; Schlinger et al., 2013). These are explosive sounds characterized by a broad frequency spectrum and lack of tonal features; they are very loud and can be heard from hundreds of meters away. A previous study using high-speed videography has shown that these sounds are produced with a very rapid upstroke motion of the wings above the back (Bostwick and Prum, 2003).

Video recordings

Video recordings were conducted in the field on three wild displaying males and on two captive juvenile non-breeding males given a silastic implant containing testosterone. These testosterone implants effectively stimulate several courtship behaviors in juvenile male and female manakins but are less effective on captive adult males (Day et al., 2006). In the field, wingsnaps were recorded with a high-speed camera (Motion Meter, Red Lake Inc., San Diego, CA, USA) at 1000 frames s^{-1}. The tripod-mounted camera was positioned 4–5 m from the center of a male's displaying court. After each recording, the video was slowed to 25 frames s^{-1} and saved on a Sony Digital Video (DV) camcorder. For captive birds, a high-speed camera (Motion Pro, Red Lake Inc.) placed 1 m from the birds was used to record video sequences at up to 2000 frames s^{-1} with Motion Pro Central software.

A stroboscopic signal produced by the Motion Meter and the Motion Pro and synchronous with the video frames (1 pulse per frame) was sent to a custom-built synchronizer and converted to a square wave. The synchronizer received a parallel signal from the trigger that marked frame 0 in the high-speed video with a high-amplitude pulse. The synchronizer sent the modified stroboscopic signal and trigger pulse to one channel of an analog (cassette) sound recorder (SonyTC-D5ProII, Sony Co.). The other channel of the cassette recorder received the birds' sounds as recorded by a Sennheiser ME-66 directional microphone. During field recording, the microphone was placed 3–6 m from the arena and recording was remotely controlled by the observer, who was hidden about 10–12 m from the arena. The distance from the microphone to the center of the male's display arena was measured with an accuracy of 5 cm and a precision of 1 cm to adjust the synchronization between sound and video (see below). When recording captive birds, the microphone was placed 18–48 cm from the center of the cage and recording was controlled from outside the room via a PC with Motion Pro Central software.

Audio-video synchronization

In the laboratory, the videos were transferred to a PC as standard AVI files. The analog audio recordings were converted to digital uncompressed PCM files (sampling rate 44.1 kHz, 16 bit). To take into account small deviations of the audio tape playback speed from the actual recording speed, all audio files were analyzed and, when necessary, edited so that the modified stroboscopic signal was exactly in phase with the strobe rate, i.e. the video frame rate. Audio and video were then synchronized with the software Adobe Premiere. To account for the delay of the audio to reach the microphone, the synchronization between the audio and the video was adjusted according to the distance between the microphone and the display bird as described above. Given that the average size of an arena is 60 cm (Fusani et al., 2007), and that birds produce wingsnaps when jumping from the perimeter perches towards the center of the arena, we estimated the distance between the microphone and the location of the wingsnap with an accuracy of <35 cm. Given that the speed of sound in air at temperatures between 20 and 35°C and relative humidity between 0 and 100% ranges from 32.2 to 35.4 cm ms^{-1}, our synchronization for field

videorecording had an accuracy of <1 ms, i.e. one video frame at 1000 frames s^{-1}. In the lab, the distance between the microphone and the position of the birds' wing was measured with an accuracy of 5 cm and precision of 1 cm, for a resulting synchronization accuracy of <0.15 ms, i.e. less than one video frame at 2000 frames s^{-1}. Synchronized videos were then analyzed with The Observer XT (v7.0, Noldus Technology).

Anatomical analysis

Anatomical observations were made on both wet (preserved) and dry skeletal specimens. Wet *M. vitellinus* specimens were obtained during field work in Panama and preserved in alcohol. Skeletal specimens were obtained from the avian collection of the Natural History Museum of Los Angeles. Anatomical terms follow those in Baumel and Witmer (1993).

RESULTS
Wing motion analysis

An early description of the movements of the wings during snap and rollsnap production was given by Bostwick and Prum (2003).
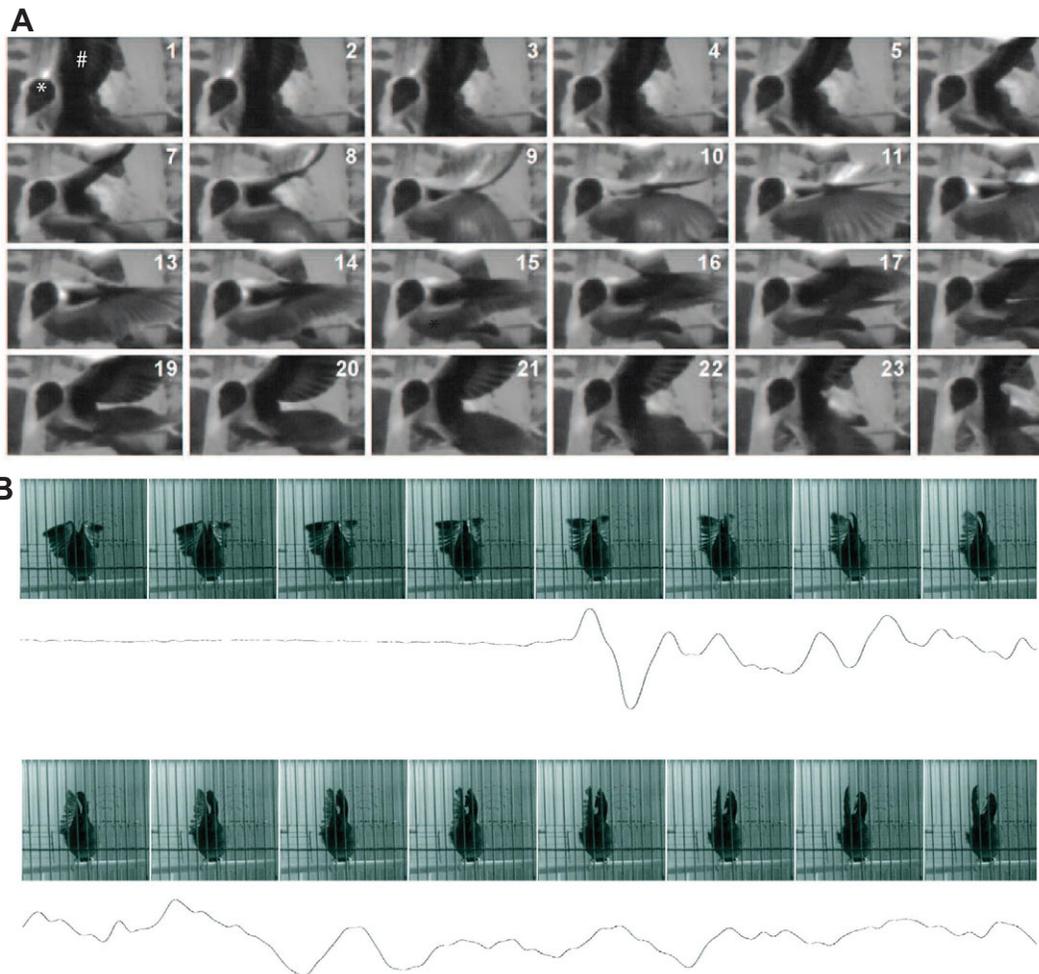

Fig. 1. High-speed video and microphone data of a manakin wingsnap. (A) A video frame series showing wing movements of a single wingsnap as observed from above. Pictured is an adult male manakin (the black cap of the crown of his head is in the left center of each frame and is indicated by an asterisk in frame 1; the bill is pointed at an angle downwards towards the bottom left corner). The wings and back also appear black; the bird's right wing is indicated by a hash in frame 1. The wings are seen moving upwards towards the camera, before colliding between frames 9 and 10 and are then retracted for the remainder of the sequence. The time between frames is 1 ms. The snap sound is produced as the radii of the wings collide between frames 9 and 10. (B) Temporally synchronized video and microphone trace (arbitrary vertical scale) for a wingsnap event. The time between frames is 1/2000 s, and increases continuously from left to right and top to bottom. The acoustic travel time delay has been removed from the audio trace.
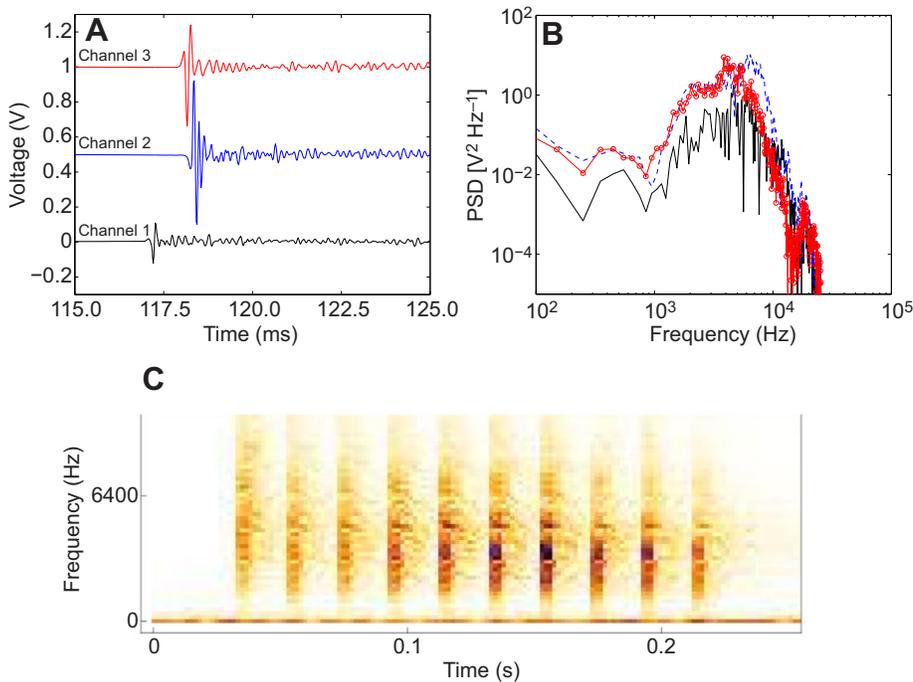
Fig. 2. Sample field data recorded for a single 'snap' event by three separate microphones. (A) Time history of a single snap. (B) Spectral content of a single snap. PSD, power spectral density. (C) Spectrogram for a series of snaps from which A and B were extracted. Data were taken with a 51,200 Hz sampling rate.

Fig. 1A is a representative video sequence captured at 1000 frames s^{-1} of an adult male performing a single wingsnap. In total, we obtained 22 video sequences from various perspectives of wild males performing single wingsnaps and rollsnaps with and without audio synchronization. Fig. 1B is a representative visual-audio sequence captured at 2000 frames s^{-1} of an individual wingsnap, with acoustic travel time delay removed from the audio trace, from a captive juvenile male performing a rollsnap. In total, we obtained video-audio synchronized recordings of 5 rollsnaps from captive testosterone-treated males facing towards or away from the camera. Because the audio recording was taken within a confined space, it differs in appearance from that measured in the field (see Fig. 2) but shows that the initial and most intense snap occurs when the wings collide.

Our high-speed video-audio synchronized recordings illustrate quite clearly that the wings collide at the upstroke of the wingsnap as described previously by Bostwick and Prum (2003). These images show that the wings initially contact on the cranial edge of the distal radius, possibly with the elbow locked (frame 9, Fig. 1A). The wings then close proximally, as the entire radii come into opposition and the patagia come into contact (frame 10, Fig. 1A). In addition, the distal ends of the wings, the carpometacarpus and digits, make contact (frames 11–14, Fig. 1A). These secondary contacts, proximal and distal to the distal radius, are less forceful than the initial contact, the force of which can be observed in the movement of the wing feathers. Prior to contact, the feathers bend smoothly backwards as the wing tips are dragged behind their insertion in the radius/ulna, the leading edge of the upward propulsion. At the moment of contact, the inertia of these feathers causes them to sharply deform (frame 5, Fig. 1A) as they maintain their upward sweep. The primary and secondary feathers continue their upward movement until they make contact in a sweeping motion as the bird retracts its wings downwards.

The hand clap analysis of Fletcher (2013) does not apply to the manakin wingsnap because, as shown in Fig. 1A, there is considerable open space between the opposing wings as they collide and they are not the nearly flat, impermeable surfaces that

are capable of ejecting air very rapidly from their enclosing space.

The wing snap mechanism by manakins also differs from that used by many pigeons and doves of the Order Columbiformes to make clapping sounds, produced as the tips of their primary feathers strike one another at the upstroke–downstroke and downstroke–upstroke transitions (Dial, 1992). The tips of the manakin primaries do not appear to make contact and only approach each after the snap is produced (Fig. 1B).

Anatomical data

Examination of the *M. vitellinus* wing revealed that the radius shows a distinctive, and seemingly unique, morphology. Because it is the radii that collide at the top of the wing stroke, we focused on this bone for our anatomical analysis. The radius is thickened distally, at the distal radio-ulnar syndesmosis (syndesmosis radioulnaris distalis) and the articulation with the radiale (articulatio radiocarpalis), where the wings initially make contact. Proximal to these articulations, the radius flattens cranio-caudally, but is

Table 1. Dimensions of the radii in the studied taxa

Taxon and number of specimens (N)	W/L	W/D
Manacus manacus (male) (N=3)	0.072±0.003	3.48±0.054
Manacus manacus (female) (N=3)	0.069±0.004	3.63±0.097
Corapipo leucochora (N=3)	0.041±0.005	1.92±0.162
Cryptopipo holochlora (N=1)	0.042	1.84
Chiroxiphia linearis (N=2)	0.045±0.0004	2.13±0.132
Pipra coronata (N=2)	0.037±0.006	1.85±0.288
Pipra erythrocephala (N=2)	0.038±0.001	1.82±0.209
Cotinga cayana (N=1)	0.0371	1.67
Sayornis nigricans (N=1)	0.0276	1.94
Taeniopygia guttata (N=1)	0.047	1.02

W/L is the width of the radius (dorso-ventral taken at mid-shaft) divided by the proximo-distal length.
W/D is the width of the radius (as for *W/L*) divided by the depth of the radius (cranio-caudal taken at mid-shaft).
Manacus measures were divided into male and female; for other taxa, samples from the two sexes were combined.

Table 2. Geometric properties of the radii for taxa examined

Taxon	Length (mm)	Width (mm)	Depth (mm)
M. manacus (male) (*N*=3)	18.0±0.48	1.30±0.04	0.38±0.07
M. manacus (female) (*N*=3)	17.7±0.23	1.22±0.06	0.34±0.02
C. leucorchoa (*N*=3)	16.8±0.19	0.69±0.09	0.36±0.02
C. holochlora (*N*=1)	22.6	0.96	0.52
C. linearis (*N*=2)	23.9±0.24	1.08±0.02	0.51±0.02
P. coronata (*N*=2)	18.8±1.7	0.69±0.04	0.38±0.04
P. erythrocephala (*N*=2)	18.3±1.5	0.69±0.04	0.39±0.06
C. cayana (*N*=1)	35.0	1.4	0.63
S. nigricans (*N*=1)	36.6	1.0	0.52

broad dorso-ventrally, giving it a board-like appearance. This is in contrast to closely related taxa (*Cryptopipo*, *Corapipo*, *Chiroxiphia* and *Pipra*; Ohlson et al., 2013), as well as various outgroups used for comparison (*Cotinga cayana*, a sister taxon to Pipridae; *Sayornis nigricans*, a suboscine passeriform; *Taeniopygia guttata*, an oscine passeriform), whose radii are less oblate in cross-section (Tables 1 and 2, Fig. 3). Also notably, both male and female manakins possess this broad radius. Females of the genus *Manacus* are known to produce wingsnaps when given androgens (Day et al., 2006), so this may be an autapomorphous trait for this taxon. Analysis of other wing-bone characteristics, such as those of the carpals, revealed nothing unique. A detailed description of other manakin skeletal characteristics is forthcoming (Friscia et al., 2016).

Field acoustic data

We were able to capture synchronous audio and video recordings showing that the initiation of the 'snap' occurs when the wings make
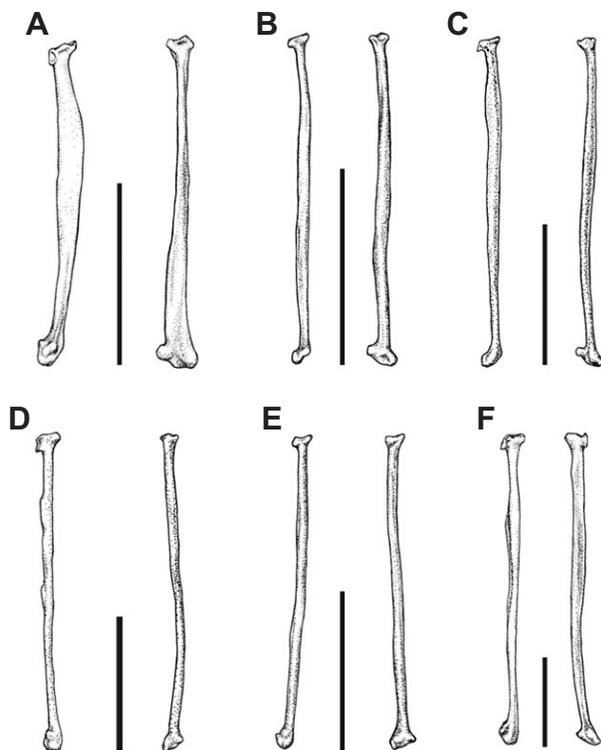

Fig. 3. Illustrations of radii of representative taxa used in this study. Each radius is shown in two views, caudal (left) and dorsal (right); proximal is toward the top of the figure. The scale bar for each pair of views is 10 mm. (A) *Manacus manacus*, (B) *Corapipo leucochora*, (C) *Cryptopipo holochlora*, (D) *Chiroxiphia linearis*, (E) *Pipra erythrocephala* and (F) *Cotinga cayana*.

contact (e.g. between frames 4 and 5 in Fig. 1B). The recording of the acoustic signal used a 44.1 kHz sampling rate whereas the time between video frames is 0.5 ms. This resolution limitation prevents a definitive assessment of contact at the moment the snap is generated. Nevertheless, the improved audio/video resolution (0.5 ms compared with 33.3 ms of the previous study by Bostwick and Prum, 2003) leads us to conclude that indeed the wing collision is the source of the wingsnap. How the sound is generated – that is, whether the source is aerodynamic or structural in origin – will be assessed by more quantitative means, as discussed next. Field acoustic data for one wingsnap event are shown in Fig. 2 for the raw microphone data, as a time trace (Fig. 2A), and the corresponding spectra (Fig. 2B). Three microphones recording simultaneously from different locations recorded one wingsnap event. The time delays are different for each microphone because of the acoustic travel time delay differences, but the spectral shapes are similar and exhibit a peak frequency around 5 kHz. As shown in Fig. 2A, the wingsnap event is an impulsive pressure wave approximately 1.5 ms long, followed by an extended lower amplitude, random-like signal. This signal is due to reflections of the wingsnap sound off environmental elements (e.g. trees) and is not part of the snap itself. Fig. 2A,B forms the basis for comparison of the three atonal sonation mechanisms evaluated. Fig. 2C includes a spectrogram of a series of 10 wingsnaps from which the data shown in Fig. 2A,B were extracted.

Quantitative evaluation of individual atonal sonation mechanisms
Wing motion kinematics

Kinematics of the wing motion for input into estimating the sound sources $Q(\mathbf{y},t)$ and $\mathbf{F}(\mathbf{y},t)$ in Eqn 1 were determined from still images obtained from the high-speed video recordings as follows. Multiple camera views were available and those aligned with the anteroposterior axis were used to determine the mean upstroke angle β(*t*) (*N*=5) while those views perpendicular to it, along the lateral axis, were used to determine the mean pronation angle θ(*t*) (*N*=4; Fig. 4). It is evident from Fig. 1B that the wing does not exhibit significant pronation until after collision, indicating that pronation cannot be a significant source of the atonal wingsnap. As a consequence, all subsequent analyses used only the upstroke angle β at a fixed pronation angle of θ=0 deg.

Fig. 5 shows the ensemble-averaged upstroke angle data as taken from three high-speed videos. The time axis has been arbitrarily shifted such that the wing motion begins at *t*=0. The data show that the stroke cycle is nearly symmetrical and requires ~20 ms for completion with little variability across birds (<5%). A Gaussian curve fit is a reasonable approximation of the measured data except for a small 0.05 rad deviation at the beginning and end of the stroke cycle. Other curve fits (linear, spline) yielded similar conclusions
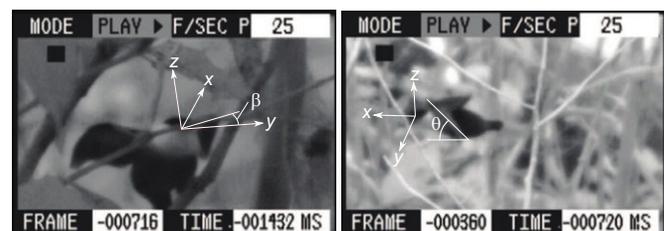

Fig. 4. Sample still images of *Manacus vitellinus* showing definition of upstroke (β) and pronation (θ) angles. Images were taken from high-speed video (500 frames s^{-1}) of manakins in the field in Panama.
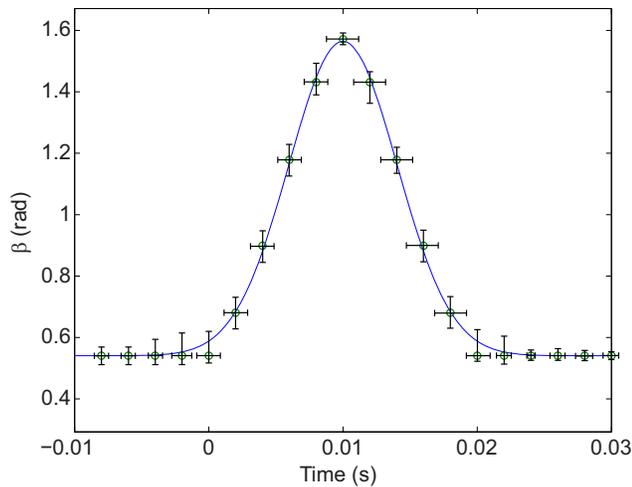
Fig. 5. Wing position as a function of time. Upstroke angle (β) data were obtained from video taken at 500 frames s^{-1}: open circles are the ensemble-averaged locations (N=5). The time and angle variability are given. Data were fitted with a Gaussian curve.

but were less convenient to use. From the kinematic data and the measured half-wing span of 11 cm, the maximum velocity at the wing tip is below 30 m s^{-1}. At the wrist, where the primary impact occurs, the velocity is approximately 10 m s^{-1} just prior to contact.

Estimates of sonation mechanisms

Before undertaking a more detailed analysis, we made initial estimates as to whether the proposed sonation mechanisms are viable, given the kinematic data. For the wingsnap of *M. vitellinus*, the peak frequency of 5 kHz corresponds to a wavelength of approximately 68 mm, which is much larger than the impact region visible in Fig. 1A,B. We thus assume that the compactness ratio ℓ/λ is small, making Eqn 1 a suitable means to estimate the sound field once the mass source and body forces are estimated from the wingsnap kinematics. If we recall the three sonation hypotheses H1–H3 discussed in the Introduction, we can immediately rule out the whip-like motion hypothesis H1 because the kinematic data show that the maximum velocity observed is 30 m s^{-1}, an order of magnitude too low to support supersonic motion.

Hypothesis H2 relies on the creation of a low pressure center that suddenly collapses. In a single-phase medium like air it is not possible to create such a scenario without an interface that separates the high pressure from the low pressure, so we conclude H2 is also not viable. This mechanism of creating an intense acoustic field is possible underwater, however, where the water–air interface permits a pressure difference to exist as used by snapping shrimp (*Alpheus heterochaelis*) to stun prey (Versluis et al., 2000).

If we reinterpret hypothesis H2 to mean that the wings create some motion of the surrounding air that causes the sonation, then we find two derivative hypotheses are feasible, associated with either the quick movement of air that is ejected between the wings (H2a) or associated with the forces created by the wing during wingsnap (H2b).

H2a: sound due to air moved by wings near contact

This hypothesis examines whether the wingsnap is created when, during upstroke and just prior to contact, the wings push the air lying between the wingtips out of the way. In this way the sonation
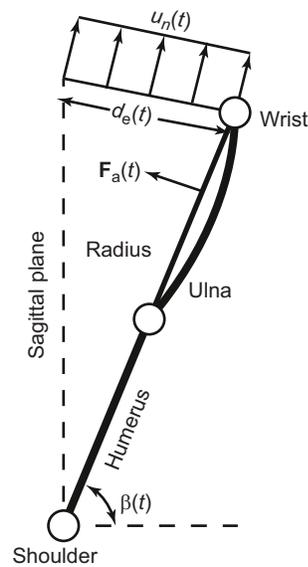

Fig. 6. Schematic diagram for the first and second sound generation mechanisms. u_n, velocity of ejected air; d_e, distance between wrist and saggital plane; $\mathbf{F}_a$, aerodynamic force applied to air by wing; β, upstroke angle; t, time.

mechanism may be modeled as the change in the mass of air contained between the approaching wings. Referring to Fig. 6, the rate at which mass leaves the region, per unit area, between the wings then leads to a sound field estimated by ρu_n, where ρ is density and u_n is the average velocity of air exiting the idealized region between one wing and the sagittal plane (the subscript n refers to the velocity component in the direction indicated in Fig. 6). Multiplying this by $2d_e$ (the distance between the wrist and the saggital plane) yields the rate at which the air is expelled, per unit depth, by the wings. The kinematic upstroke data give $d_e(t)$=tan[(π/2 −β)]w, where w is the distance from the shoulder to the wrist. The velocity $u_n(t)$ can be estimated using the fact that, for constant density air, the mass that leaves must be proportional to the change in the area $A(t)$ enclosed between the wing and the sagittal plane. From this idea it follows that:

$$u_n(t) = -\frac{1}{d_e}\frac{\mathrm{d}A}{\mathrm{d}t},\tag{3}$$

and A is known from the geometry in Fig. 6. Using the kinematic upstroke data, it follows that $Q(\mathbf{y},t)$ in Eqn 1 equal to $\rho u_n d_e$ per unit
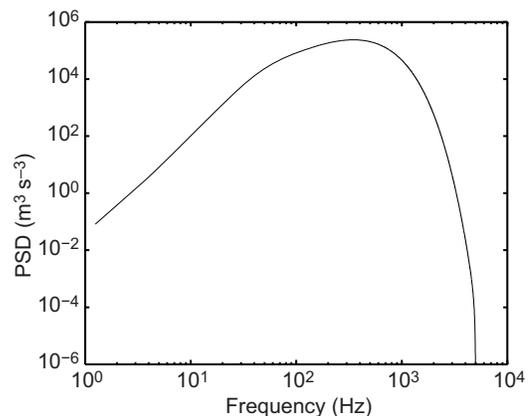

Fig. 7. Spectrum of the aeroacoustic source term $Q(\mathbf{y},t)$ of hypothesis H2a.

depth yields a sound field with spectrum shown in Fig. 7 that peaks near 400 Hz, a full order of magnitude lower than the field-measured acoustic data. The same estimate during the downstroke portion applies, with only a change in sign from dA/dt becoming positive, leading to only a change in sign of $p'(\mathbf{x},t)$. From this argument, we conclude that the 'jetting' of air away from *M. vitellinus* by the wings just prior to contact cannot explain the measured acoustic data.

H2b: sound due to forces during wingsnap

This sonation hypothesis examines whether wingsnaps result from unsteady forces of the wings, with Q=0 signifying no sources of mass. The idea and analysis are very similar to those of noise due to rotating propellers; any unsteady force creates sound. From Eqn 1, the kinematics are now used to estimate $\mathbf{F}(\mathbf{y},t)$ during the upstroke and downstroke motions. To use the second term in Eqn 1, one must know both $\mathbf{F}$ and r. The latter is relatively easy as it can be considered fixed to the wing at roughly 80% of span from the shoulder to the wrist (Mueller, 2001; see Fig. 6). Thus r is a purely kinematic quantity and is related to the upstroke angle β. The force $\mathbf{F}$ is less trivial as it lumps together several aerodynamic forces found in the unsteady motion of a wing at low Reynolds number, a topic of active research (Dickinson et al., 1999; Mueller, 2001; Sane and Dickinson, 2001; Miller and Peskin, 2005; Azuma, 2006; Shyy et al., 2008). These references show that the coordination between translation and rotation of a wing have dramatic impact on the resulting force, and quantitatively predicting the aerodynamic forces as a function of the wing kinematics is challenging.

Without knowing the force magnitude, we may easily estimate the unsteadiness in the force. During the wingsnap of *M. vitellinus*, the bird may be perched without any forward motion and no measurable pronation (see Fig. 6). The aerodynamic forces are then directly proportional to the wing's acceleration during the upstroke and downstroke motions, d^{2}β/dt^2, and always oriented in the direction perpendicular to the wing. From this information and Eqn 1, one finds the pressure spectrum must be proportional to the spectrum of the third time derivative of β(t) whose spectrum peaks at a frequency around 100 Hz (not shown). This frequency is substantially lower than the measured value of 5 kHz, implying that this mechanism is also inconsistent with the measured acoustic data. *Manacus vitellinus* are unable to move their wings fast enough to aerodynamically create the atonal wingsnap sonation.

H3: vibration-induced sound caused by wing–wing impact

None of the purely aerodynamic hypotheses (H1, H2, H2a, H2b) are consistent with the measured spectrum of wingsnaps because the underlying wing kinematics do not have the proper time scale; the wings move too slowly to create the measured sound. Thus, another mechanism must be examined that has a smaller inherent time scale.

The high-speed videos (see Fig. 1A, frame 9) demonstrate that the wings impact in the sagittal plane and support the H3 hypothesis, i.e. that a sound-generating collision process may occur, much like the sound created when one stick strikes another. The impact happens very quickly, in a length of time shorter than the interval between two subsequent frames collected at 2000 frames s^{-1}, i.e. 0.5 ms. After the initial impact, the wings remain in contact in the sagittal plane (Fig. 1A, frames 10–14) and then pronate before the downstroke is initiated (Fig. 1A, frame 15). The frames of Fig. 1A show that the collision occurs at the cranial edge of the distal radius and we hypothesize that this collision causes the bones within the wing to vibrate and generate sound. Because there is no evidence of stridulation in the wingsnap, where the rubbing could cause a torque

to be applied to the radii, it is unlikely that significant torsional motion is created, so we focused on transverse vibrations rather than torsional vibrations.

To estimate the sound created by the collision, elastic properties of avian bone [with a density of solid bone, ρ_s, of 1800±200 kg m^{-3} (Dumont, 2010) and elastic modulus, E, of 12±1 GPa (Reed and Brown, 2001)] and geometric properties of the *M. vitellinus* radius (Table 2) were used to calculate the fundamental frequencies associated with the impact, as follows. Prior to the collision, the outer wing's inertia and aerodynamic resistance help set the velocity of the wings just prior to contact, as recorded in the kinematic data, which is of the order of 10 m s^{-1} at the wrist. In principle, the radius, ulna and humerus can all participate in wingsnap sound generation. The video frames in Figs 1 and 4 indicate that during a wingsnap, *M. vitellinus* locks its elbow to create a solid connection between the humerus and the radius and ulna. However, the anatomy of the elbow serves to isolate the humerus from the radius and ulna such that it is unlikely to vibrate with any significant strength to contribute to the wingsnap. In addition, the videos also indicate that the primary collision occurs between radii, leaving the ulna as a passive element and also unlikely to contribute to the radiated sound. The sound thus appears to be primarily generated by the radius-on-radius collision.

To evaluate whether the direct radius-on-radius impact creates sounds that scale with predicted natural vibrational frequencies of the bone itself, we first constructed a crude model of the radius vibration. We modeled the radius as being fixed (i.e. clamped) at the elbow and free at the wrist. The aspect ratio of the radius is greater than 10 so we treat it as a Bernoulli–Euler beam (Graff, 1991) of uniform properties. For a free-clamped beam, the nth fundamental lateral vibration frequency is:

$$f_n = \frac{(\beta_n L)^2}{2\pi L^2}\sqrt{\frac{EI}{\rho_s A}}, \tag{4}$$

where $\beta_n L$ solves the eigenvalue problem $\cos(\beta L)\cosh(\beta L)=-1$ (where L is the length of the Bernoulli–Euler beam) and has the values $\beta_1 L$=1.875, $\beta_2 L$=4.694 and $\beta_3 L$=7.855 for the first three modes of vibration. The moment of inertia I and radius cross-sectional area A are taken as those of a uniform elliptical cylinder using the properties in Table 2. The first three corresponding frequencies, which represent averages over the (N=3) samples in Table 1 (with range in parentheses), are approximately 800 Hz (±200 Hz), 5.5 kHz (±1 kHz) and 14.7 kHz (±1.5 kHz). Because our data do not take into account the damping of fleshy and feather material surrounding the bone, these estimates are likely high, but by an unknown amount. Nevertheless, these fundamental frequencies are of the correct order of magnitude so it is plausible that the contact-induced sound produces the measured signal.

Though the collision-as-wingsnap hypothesis is plausible, we must examine it in more detail as not all vibration frequencies that are possible will be able to effectively generate sound (Goldstein, 1976). Using the video frame shown in Fig. 8A as a guide, we constructed an analytical model of one radius being impacted by the other and then evaluated it numerically. To develop a more quantitative prediction of the sound we must link the motion of the wing, a complex physical structure with both 'stiff' (i.e. bone) and 'fleshy' (i.e. muscle, tissue, feather, etc.) elements, to the sound it creates upon impact. To do this, we replaced the radii of the two wings with simple beams of elliptical cross-section that are fixed at the elbow and free at the wrist, as described earlier. Geometrical symmetry allows the two-element model (Fig. 8B) to be simplified
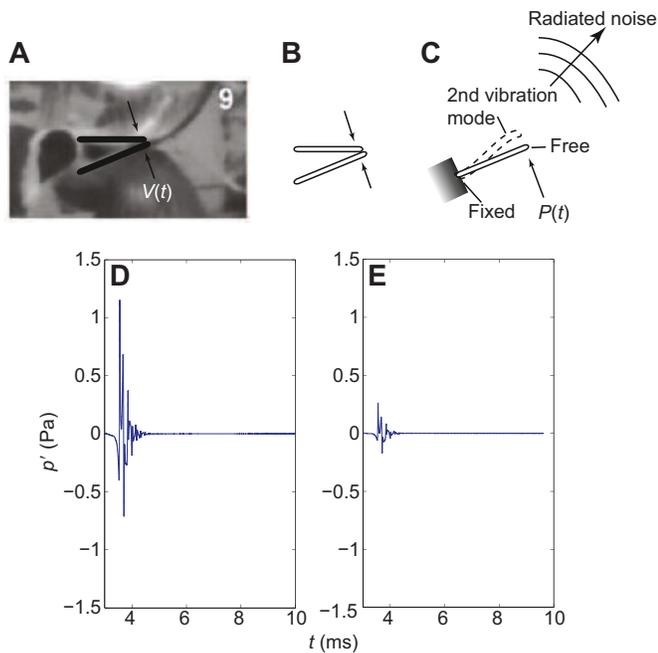
Fig. 8. Construction and prediction of impact hypothesis H3.
(A–C) Schematic diagram of (A) the alignment of the engineering model, (B) isolated elements at collision and (C) the engineering model of single element showing applied load, deflected state and resultant sound. V, velocity magnitude of wrist towards the saggital plane; P, load. (D,E) Predicted pressure trace (p') based on a vibrating beam model of the wingsnap-as-collision atonal sonation. Numerical parameters were damping parameter $\delta=1\times10^4$ s^{-1} and collision time scale $\tau_c=2\times10^{-3}$ s (D), and $\tau_c=2\times10^{-4}$ s (E).

to a single-element model where the effect of one radius on the other is to impart a load $P(x,t)$, where x is the spatial coordinate along the radius and t is time, that initiates the vibrations that eventually lead to the sound. We assume that the collision-generated sound is sufficiently weak to be neglected when determining the motion of the radius so that we can break the analysis into two parts: first we need to determine the transverse deformation $\eta(x,t)$ of the idealized radius, which varies along the length of the radius and with time, due to the imposed load $P(x,t)$ and then determine the radiated sound $p'(\mathbf{x},t)$ from the collision-induced vibrational motion of the radius.

Details of the model (including references) are given in Appendix 1 but the main points are summarized here. To determine the deflection of the radius, a one-dimensional dynamical model is constructed that links the impact load $P(x,t)$ to the transverse vibration of the beam $\eta(x,t)$ through the application of Newton's second law of motion to a slender beam with clamped-free boundary conditions. The dynamic model also includes damping arising from the 'fleshy' physiology of the wing (e.g. muscles, feathers, etc.) that can absorb some of the vibrations. The damping parameter δ is unknown. A Hertzian model of the impact is used to approximate $P(x,t)$ as a Gaussian function in time and localized at the wrist, with unknown collision time scale τ_c. For each pair of values of (δ, τ_c) the resulting partial differential equation that models the collision-induced vibration is solved using the finite element technique to give the solution $\eta(x,t)$.

The sound generated by the vibration of the radius is then estimated by solving the so-called wave equation associated with the propagation of sound in still air by requiring the velocity of the fluid adjacent to the bone to be equal to the velocity of the bone itself. The sound heard at the microphone located at point x, $p'(\mathbf{x},t)$, is then

directly linked to the transverse vibration $\eta(x,t)$ as shown in Eqn A7 of Appendix 1.

Because we do not know the damping parameters and collision time scale, a series of results using different combinations of (δ, τ_c) were created and compared against the field-measured microphone signal. The details of our estimation are shown in Appendix 2. Focusing on the waveform in Fig. 8, we found that the selected parameters ($\delta=10^4$ s^{-1} and 2×10^{-4} s$\leq\tau_c\leq2\times10^{-3}$ s) yield an overall duration of the sonation of roughly 1–1.5 ms and are characterized by 2–5 significant peaks with a 'wave packet' envelope. The predicted sonations are very quiet after the primary sonation while the field data are subject to background noise and reflections and show more fluctuations after the primary sonation. From the figures, we infer that a time scale of 2×10^{-4} s$\leq\tau_c\leq2\times10^{-3}$ s best matches the experimental acoustic data.

Although our model can predict the main features of the wingsnap, there are residual differences between the predicted time histories in Fig. 8D,E and the field data in Fig. 2 that arise because our idealized model does not include the full complexity of the actual sonation. For example, the video data suggest that the radii are critical to the wingsnap but they do not permit definitive conclusion that the humerus and ulna do not contribute to the wingsnap; our model confirms that the inter-radii collision hypothesis is sufficient to explain the dominant features of the atonal sonation wingsnap but would need modification to include other skeletal contributions. Furthermore, the model's approximation of the vibration damping that occurs within the wing during wingsnap necessarily ignores all of the complexities associated with structural vibrations in, and sound propagation through, a bird wing.

DISCUSSION
The above analysis reveals that the radii bones of *M. vitellinus* are morphologically specialized relative to those of related bird species and the *M. vitellinus* wingsnap is produced as these radii collide with one another at the apex of the upstroke above the bird's back. Indeed, the only sonation mechanism quantitatively consistent with the measured recordings of a wingsnap depends on the impact of the wings directly above the body. Previously proposed aerodynamic mechanisms depend on the kinematics of the wings and are too slow relative to the 5 kHz peak observed. The percussion, or contact, hypothesis introduces a shorter time scale associated with the vibration modes of the radius bone. Damping of this collision-induced vibration by the fleshy material and feathers found on the wing yields the ultimate acoustic signature of the wingsnap.

Production of wingsnaps by species of the genus *Manacus* is associated with specializations of their radii bones that in all likelihood contribute to the spectral and temporal properties of their snaps. Skeletal adaptations have been described in other manakin species [K. E. Bostwick, Phylogenetic analyses of the evolution of behavior, wing morphology, and the kinematics of mechanical sound production in the neotropical manakins (Aves: Pipridae), PhD thesis, University of Kansas, 2002; Bostwick et al., 2012], suggesting a unique degree of phylogenetic developmental plasticity in bone growth in this bird family. Male manakins also exhibit specializations of several muscles used to lift and retract the wings (Lowe, 1942; Schultz et al., 2001). Flight is the primary mode of locomotion by manakins; thus – assuming the presence of trade-offs in these adaptations – these musculoskeletal adaptations probably hinder efficient flight biomechanics. When unusual phenotypic traits evolve in only one sex under sexual selection pressure, they are thought to carry costs that may become the target of mate choice (Zahavi, 1975). Both male and female golden-

collared manakins possess radii bones that are unusually flattened and an anecdotal report of a wild female manakin wing-snapping near the nest (M.W., unpublished observations) suggests females may naturally wingsnap, perhaps in predator deterrence or nest defense. Snapping behavior may have then secondarily been incorporated into the male's courtship display; similar processes have been described in other species (Tinbergen, 1952).

Non-vocal sound production is widespread throughout the animal kingdom and, in birds, the behavioral mechanisms producing sonations are diverse (e.g. Bostwick and Prum, 2003, 2005; Bostwick et al., 2010; Clark and Feo, 2008). In many species, non-vocal sounds arise from air passage over specialized wing and tail feathers (e.g. Clark and Feo, 2008). Early observations of sex differences in the manakin wing feathers led to speculation that the wingsnaps were produced by collision of the feathers (Chapman, 1935). We now know that females can produce wingsnaps when stimulated with testosterone (Day et al., 2006, 2007), arguing against sexually dimorphic feather structure as a source of the wingsnap.

The degree to which bone-on-bone collisions are used to create sounds is unknown, but they are likely to occur only in species possessing bony structures with minimal damping properties of skin, feathers and muscle. High-amplitude non-vocal signals involving specialized skeletal structures are present in other avian taxa, notably the woodpeckers (*Picoides*). These birds hammer with extraordinary force (G-forces of ca. 1200, enough to give most vertebrates a strong concussion; Yoon and Park, 2011) against wood for purposes of feeding and to communicate via high-amplitude acoustic signals (Bent, 1939), but specializations of their skulls prevent damage to the brain (Wang et al., 2011).

Although the *Manacus* species stand out for the amplitude of their wing sounds (Chapman, 1935), other avian species produce snap-like sounds, including other species of manakins (Bostwick and Prum, 2003) as well as some larks and cisticolas (e.g. Norberg, 1991). Although some of these sonations are clearly not produced by a wing collision mechanism (Bostwick and Prum, 2003), it is possible that similar bone-on-bone collisions are utilized by other species. Undoubtedly, additional behavioral and anatomical study, including the application of quantitative physical (modeling) approaches, will identify novel mechanisms for sound production in birds and in other animal species.

Conclusions

Through application of elementary aeroacoustic theory, we suggest that the wingsnap sonation mechanism of male golden-collared manakins (*M. vitellinus*) is caused by the percussive collision of the wings during their quick upward wing stroke. High-speed synchronous video and audio recordings showed that the noise was generated during the interval when the morphologically unique radii bones collide. The collision resulted in a transient snap-like sound with a peak frequency of approximately 5 kHz. Using the kinematic data from the video, a motion model of the wings was constructed and used to assess previously proposed atonal sonation mechanisms. The motion of the wings yields a maximum velocity of 30 m s^{-1} and sounds generated by aerodynamic means generate acoustic frequencies of the order of 100–400 Hz. In contrast, a wing collision mechanism introduces a shorter time scale associated with the vibration of the underlying radius that occurs at higher frequencies. When coupled to a vibration-induced sound formulation with significant structural damping, a spectral and temporal waveform prediction is possible that is consistent with the

experimental data, with a peak frequency of approximately 5–7 kHz and transient duration of 1–1.5 ms.

Appendix 1: wing-impact vibration model

The collision-as-wingsnap mechanism involves (1) the creation of structural vibrations and (2) the subsequent radiation of sound, as sketched in Fig. 8. To determine the motion of the modeled radius, which is fixed at the elbow and free at the wrist, we assume that the deflection is governed by the one-dimensional Bernoulli–Euler beam (Graff, 1991) equation:

$$\frac{\partial^2}{\partial x^2}\left(EI\frac{\partial^2 \eta}{\partial x^2}\right) + \delta\rho_s A\frac{\partial \eta}{\partial t} + \rho_s A\frac{\partial^2 \eta}{\partial t^2} = P(x,t), \qquad (A1)$$

which relates the transverse deflection $\eta(x,t)$ of the bone to the unsteady applied load $P(x,t)$ subject to the boundary conditions:

$$\partial^2 \eta/\partial x^2 = 0$$
$$\partial^3 \eta/\partial x^3 = 0$$

at the free end, and:

$$\eta = 0$$
$$\partial \eta/\partial x = 0 \qquad (A2)$$

at the fixed end, where the position x is taken along the radius. The product EI (where E is elastic modulus and I is the moment of inertia) is taken as constant along the length using data from Table 1, and the radius starts at rest, $\eta(x,0)=0$. The second term of Eqn A1 is an approximate form of structural damping due to Rayleigh (Graff, 1991) and models the vibration absorption effect caused by the 'fleshy' parts of the wing; δ is a coefficient proportional to the amount of damping as discussed in Results. Its value is not known and must be determined using experimental data.

The vibration is hypothesized to be due to contact between the bird's two radii, which is modeled via the applied load $P(x,t)$. While there is incomplete physiological information to know precisely what the structural properties are at the point of impact, we can apply a simple elastic dynamic impact model, originally introduced by Hertz (Johnson, 1985), which replaces the radius-on-radius impact with a simple applied load as:

$$P(x,t) = A\exp\left(-\frac{(t-t_c)^2}{\tau_c^2}\right), \qquad (A3)$$

where A is the amplitude, t_c is the time of collision and τ_c is the collision time constant. Neither A nor t_c is important as they control the overall amplitude and delay time but do not affect the spectrum. (Note: we estimate A based on the kinematic data and a mass estimate of the wing.) The collision time constant, τ_c, is, however, more critical as it controls the time scale of the collision. From the video analysis, the collision time occurs between two consecutive frames, such as between two consecutive frames at 2000 frames s^{-1} (Fig. 2); thus, $\tau_c<0.5$ ms.

According to the Hertz impact model, τ_c is related to the elastic material properties and boundary conditions of the underlying structure. To minimize the complexity of this system, we selected a reasonable minimum value, say τ_{min}, representing the shortest contact time plausible for the collision. This estimate is based on the time taken for the impact wave to travel from the point of impact through the thickness of the radius across the bone and return. For

our elliptical model we have:

$$\tau_{min} = \frac{2D_{eff}}{\sqrt{E/\rho_s}} \approx 2 \times 10^{-6}\text{s}, \qquad (A4)$$

where $D_{eff} = \sqrt{WD}$ is the hydraulic diameter of the radius, for the values listed in Table 1. Using this value as a minimum, we solved for the displacement $\eta(x,t)$ using Eqn A1 for τ between 2×10^{-6} and 2×10^{-3} s. Convergence tests were done (not shown) to ensure the numerical solution to Eqn A1, subject to the boundary conditions in Eqn A2, was grid and time-step independent.

With the displacement $\eta(\mathbf{x},t)$ known, we can now determine the pressure disturbances in the air created by the vibrating radius. It is known from aeroacoustics (Goldstein, 1976) that the motion of the surface of a structure couples to the fluid through the boundary condition:

$$\rho \frac{\partial^2 \eta}{\partial t^2} = -\frac{\partial p'}{\partial n}, \qquad (A5)$$

where n is the coordinate perpendicular to the bone. In the fluid the pressure fluctuations, $p'(\mathbf{x},t)$ is accurately described by the wave equation:

$$\frac{1}{c^2}\frac{\partial^2 p'}{\partial t^2} - \left(\frac{\partial^2 p'}{\partial x^2} + \frac{\partial^2 p'}{\partial y^2} + \frac{\partial^2 p'}{\partial z^2}\right) = 0. \qquad (A6)$$

Approximate analytical solutions of the wave equation, Eqn A6, subject to the boundary condition Eqn A5 for a finite-length elliptical cylinder are given by Maillard (J. Maillard, Advanced time domain sensing for active structural acoustic control, PhD thesis, Virginia Polytechnic Institute and State University, 1997), where the elliptical cross-section is replaced by a circular one and where it is assumed that the vibrating element is placed midway along an infinitely long, non-vibrating baffle. Then, the radiated sound at this point due to a specified distribution of transverse acceleration is:

$$p'(R, \theta, \phi, t) = -\frac{\rho}{2\pi^2 \sin\theta} \int_{-\infty}^{+\infty} \frac{1}{kR} \sum_{n=0}^{\infty} \frac{\exp(-ikR)\ i^{n+1}}{[H_n^{(2)}(kD_{eff}\sin\theta)]'}, \qquad (A7)$$

$$\omega^2 \hat{\eta}(\omega)\cos(n\phi)\exp(-i\omega t)\,\mathrm{d}\omega$$

where (R, θ, ϕ) is the location of the microphone in spherical coordinates, $H_n^{(2)}$ is the Hankel function of order n of the second kind, and $\hat{\eta}(\omega)$ is the time-Fourier transform of $\eta(t)$. In Eqn A7, we have neglected any field dependence on $\sin(n\phi)$ because of geometric symmetry; the original derivation by Maillard includes both. The acoustic wave number k is given by $k=\omega/a_\infty$.

All of the predictive elements have now been described and, with them, the procedure used to estimate the sound created during wingsnaps is as follows. Values for the damping δ and collision time constant τ_c are selected and a solution for $\eta(\mathbf{x},t)$ is obtained from the finite element solution of Eqn 2. The acoustic field is estimated from Eqn A7 to find $p'(\mathbf{x},t)$ from the integral over ω. With $p'(\mathbf{x},t)$ known, the microphone recordings can be predicted and their spectra computed, and both are compared with data in Fig. 4.

Appendix 2: estimation of the damping and collision constant

The time history of the predicted sound, and the corresponding frequency spectrum, of a set of candidate estimates were created using the range of parameters of 2×10^{-6} s$\leq\tau_c\leq2\times10^{-3}$ s and a large range of damping values 1×10^{-1} s$\leq\delta\leq1\times10^5$ s^{-1}. From this range,

the radiated pressure field was determined and visually compared with the experimental data of Fig. 4. Samples of the corresponding spectra are shown in Figs S1 and S2 for variable damping and contact time constants, respectively. To determine the 'best' estimate of δ and τ_c, the following two criteria were used: (1) the peak predicted frequency must be of the same order as that measured (i.e. 5 kHz); and (2) the temporal signal must have the same duration and qualitative signature as that measured.

The results of Figs S1 and S2 were then compared with the field data of Fig. 3. Because the microphones were not calibrated, the comparison is only relative and is based on the shapes of the spectra. Considering Fig. S1, at damping levels $\delta\leq1\times10^3$ s^{-1}, the predicted spectra show a tonal quality associated with the fundamental modes of the vibrating bone and are rather unlike the measured spectrum. Because the role of damping in the model is to mimic the internal losses during vibration, as due to the 'fleshy' elements of the wing, it is perhaps not surprising that larger damping values are required. The data suggest that values of δ at least of the order of 10^4 s^{-1} are required to remove the tonality.

The effect of the collision time constant τ_c is shown in Fig. S2. Here, it can be seen that slower collision times are more representative. At time scales less than or equal to 10^{-5} s, the high-frequency vibration modes are more strongly excited and produce a more tonal spectrum than measured. At higher damping rates, the spectral peaks are removed, leaving a spectrum that peaks around 8–10 kHz (not shown). While such a spectrum is plausible, it seems highly unlikely that the proper collision time scale is 2 µs given the fleshy and feather material surrounding the contacting radii. Thus, collision time constants of the order of 1–10 µs were deemed unrealistic.

Supplementary information
Supplementary information available online at
http://jeb.biologists.org/lookup/suppl/doi:10.1242/jeb.128231/-/DC1

References
Azuma, A. (2006). *The Biokinetics of Flying and Swimming*, 2nd edn. Reston, VA: American Institute of Aeronautics and Astronautics.

Baumel, J. J. and Witmer, L. M. (1993). *Osteologia*. In *Handbook of Avian Anatomy: Nomina Anatomica Avium* (ed. J. J. Baumel), pp. 45-132. Cambridge, MA: Nuttal Ornithological Club.

Bent, A. C. (1939). *Life Histories of North American Woodpeckers, Order Piciformes. Smithsonian Institution United States National Museum Bulletin, No. 174.* Washington, DC: United States Government Printing Office.

Bostwick, K. S. and Prum, R. O. (2003). High-speed video analysis of wing-snapping in two manakin clades (Pipridae: Aves). *J. Exp. Biol.* **206**, 3693-3706.

Bostwick, K. S. and Prum, R. O. (2005). Courting bird sings with stridulating wing feathers. *Science* **309**, 736.

Bostwick, K. S., Elias, D. O., Mason, A. and Montealegre-Z, F. (2010). Resonating feathers produce courtship song. *Proc. R. Soc. B Biol. Sci.* **277**, 835-841.

Bostwick, K. S., Riccio, M. L. and Humphries, J. M. (2012). Massive, solidified bone in the wing of a volant courting bird. *Biol. Lett.* **8**, 760-763.

Chapman, F. M. (1935). The courtship of Gould's manakin (*Manacus vitellinus vitellinus*) on Barro Colorado Island, Canal Zone. *Bull. Am. Mus. Nat. History* **68**, 472-521.

Clark, C. J. and Feo, T. J. (2008). The Anna's hummingbird chirps with its tail: a new mechanism of sonation in birds. *Proc. R. Soc. B Biol. Sci.* **275**, 955-962.

Day, L. B., McBroom, J. T. and Schlinger, B. A. (2006). Testosterone increases display behaviors but does not stimulate growth of adult plumage in male golden-collared manakins (*Manacus vitellinus*). *Horm. Behav.* **49**, 223-232.

Day, L. B., Fusani, L., Hernandez, E., Wise, P. M. and Schlinger, B. A. (2007). Testosterone and its effects on courtship in golden-collared manakins: seasonal, sex and age differences. *Horm. Behav.* **51**, 62-68.

Dial, K. P. (1992). Activity patterns of the wing muscles of the pigeon (*Columba livia*) during different modes of flight. *J. Exp. Zool.* **262**, 357-373.

Dickinson, M. H., Lehmann, F.-O. and Sane, S. P. (1999). Wing rotation and the aerodynamic basis of insect flight. *Science* **284**, 1954-1960.

Dumont, E. R. (2010). Bone density and the lightweight skeletons of birds. *Proc. R. Soc. B Biol. Sci.* **277**, 2193-2198.

Fletcher, N. H. (2013). Shock waves and the sound of a hand-clap – a simple model. *Acoust. Aust.* **41**, 165-168.

Friscia, A. R., Sanin, G. D., Lindsay, W. R., Day, L. B., Schlinger, B. A., Tan, J. and Fuxjager, M. J. (2016). Adaptive evolution of a derived radius morphology in manakins (Aves, Pipridae) to support acrobatic display behavior. *J. Morphol.* doi:10.1002/jmor.20534.

Fusani, L., Giordano, M., Day, L. B. and Schlinger, B. A. (2007). High-speed video analysis reveals individual variability in the courtship displays of male golden-collared manakins. *Ethology* **113**, 964-972.

Goldstein, M. E. (1976). *Aeroacoustics*. New York, NY: McGraw-Hill.

Graff, K. F. (1991). *Wave Motion in Elastic Solids*. Mineola, NY: Dover Publications, Inc.

Johnsgard, P. A. (1994). *Arena Birds: Sexual Selection and Behavior*. Washington, DC: Smithsonian Institution Press.

Johnson, K. L. (1985). *Contact Mechanics*. Cambridge: Cambridge University Press.

Lowe, P. R. (1942). The anatomy of Gould's manakin (*Manacus vitellinus*) in relation to its display. *Ibis* **6**, 50-83.

Lowson, M. V. (1965). The sound field for singularities in motion. *Proc. R. Soc. Lon. A Math. Phys. Eng. Sci.* **286**, 559-572.

Miller, L. A. and Peskin, C. S. (2005). A computational fluid dynamics of 'clap and fling' in the smallest insects. *J. Exp. Biol.* **208**, 195-212.

Morse, P. M. and Ingard, K. U. (1968). *Theoretical Acoustics.* Princeton, NJ: Princeton University Press.

Mueller, T. J. (ed.) (2001). Fixed and flapping wing aerodynamics for micro air vehicle applications. In *Progress in Astronautics and Aeronautics*, Vol. 195. Reston, VA: American Institute of Aeronautics and Astronautics.

Norberg, R. A. (1991). The Flappet lark *Mirafra rufocinnamomea* doubles its wingbeat rate to 24 Hz in wing-clap display flight: a sexually selected feat. *J. Exp. Biol.* **159**, 515-523.

Ohlson, J. I., Irestedt, M., Ericson, P. G. P. and Fjeldså, J. (2013). Phylogeny and classification of the New World suboscines (Aves, Passeriformes). *Zootaxa* **3613**, 1-35.

Prum, R. O. (1998). Sexual selection and the evolution of mechanical sound production in manakins (Aves: Pipridae). *Anim. Behav.* **55**, 977-994.

Reed, K. L. and Brown, T. D. (2001). Elastic modulus and strength of emu cortical bone. *Iowa Orthop. J.* **21**, 53-67.

Riede, T. and Goller, F. (2010). Peripheral mechanisms for vocal production in birds —differences and similarities to human speech and singing. *Brain Lang.* **115**, 69-80.

Sane, S. P. and Dickinson, M. H. (2001). The control of flight force by a flapping wing: lift and drag production. *J. Exp. Biol.* **204**, 2607-2626.

Schlinger, B. A., Barske, J., Day, L., Fusani, L. and Fuxjager, M. J. (2013). Hormones and the neuromuscular control of courtship in the golden-collared manakin (*Manacus vitellinus*). *Front. Neuroendocrinol.* **34**, 143-156.

Schultz, J. D. and Schlinger, B. A. (1999). Widespread accumulation of [3H] testosterone in the spinal cord of a wild bird with an elaborate courtship display. *Proc. Natl. Acad. Sci. USA* **96**, 10428-10432.

Schultz, D. J., Hertel, F., Bauch, M. and Schlinger, B. A. (2001). Adaptations for rapid and forceful contraction in wing muscles of the male golden-collared manakin: sex and species comparisons. *J. Comp. Physiol. A Sens. Neural. Behav. Physiol.* **187**, 677-684.

Shyy, W. Y., Lian, Y., Tang, J., Viieru, D. and Liu, H. (2008). *Aerodynamics of low Reynolds number flyers*. Cambridge: Cambridge University Press.

Skutch, A. F. (1969). Life histories of Central American birds. III. *Cooper. Ornithol. Soc. Pacific Coast Avif.* **35**, 1-580.

Snow, D. W. (1962). A field study of the black and white manakin, *Manacus manacus*, in Trinidad. *Zoologica* **47**, 65-104.

Tinbergen, N. (1952). Derived activities; their causation, biological significance, origin, and emancipation during evolution. *Quart. Rev. Biol.* **27**, 1-32.

Versluis, M., Schmitz, B., von der Heydt, A. and Lohse, D. (2000). How snapping shrimp snap: through cavitating bubbles. *Science* **289**, 2114-2117.

Wang, L., Cheung, J. T.-M., Pu, F., Li, D., Zhang, M. and Fan, Y. (2011). Why do woodpeckers resist head impact injury: a biomechanical investigation. *PLoS ONE* **6**, e26490.

Yoon, S.-H. and Park, S. (2011). A mechanical analysis of woodpecker drumming and its application to shock-absorbing systems. *Bioinspir. Biomimet.* **6**, 016003.

Zahavi, A. (1975). Mate selection – a selection for a handicap. *J. Theor. Biol.* **53**, 205-214.